Int. J. Heat Mass Transfer. Vol. 35, No. 4, pp 861–875, 1992
Printed in Great Britain

0017–9310/92 $5.00+0.00

Transient natural convection of water near its density extremum in a rectangular cavity

S. L. BRAGA and R. VISKANTA
Heat Transfer Laboratory, School of Mechanical Engineering, Purdue University, West Lafayette, IN 47907, U.S.A.

(*Received* 24 *September* 1990 *and in final form* 2 *April* 1991)

Abstract—An experimental and theoretical investigation of transient natural convective heat transfer to water near its maximum density in a rectangular cavity is reported. Different temperatures are imposed on the opposing vertical walls, and the effects of density inversion of water that has its maximum density at about 4°C are investigated. Initially, the fluid inside the test cell is at a uniform temperature, and then the temperature of one of the cold vertical walls is suddenly lowered and kept at 0°C. The hot wall is maintained at a constant temperature during the course of each experiment and is equal to the initial temperature of the water that varies from 8 to 20°C. Solutions of the governing equations are obtained numerically for all experiments discussed. Photographs of flow visualization and predictions of the flow patterns as well as a comparison of measured and calculated temperatures are presented. From the results obtained it is demonstrated that the density inversion of water has a great influence on the natural convection in the cavity, and the flow structure cannot be predicted using the classical natural convection models which employ the Boussinesq approximation.

INTRODUCTION

NATURAL convection in enclosures has been studied both experimentally and theoretically by numerous investigators. Most of the studies are concerned with fluids for which density decreases linearly with increasing temperature, and the Boussinesq approximation is valid. However, many fluids exhibit an extremum in the density–temperature relationship. Water is the most important example, but others such as molten bismuth, antimony, gallium and tellurium can be cited [1]. Due to the effect of density inversion, the natural convective motion, near to the density extremum, develops in a complicated manner.

Several numerical studies have been reported in the literature concerning the convective flow in a variety of cavities having different types of boundary conditions. Investigations for steady-state [1–7] and transient [8–12] natural convection conditions revealed that the flow structure and the heat transfer are strongly influenced by the density inversion.

A number of experimental studies which were concerned with natural convection flow of water in a temperature range where the density inversion of water is present have been published [13–16]. Cheng *et al.* [13] studied the effects of natural convection on ice formation around an isothermal, cooled horizontal cylinder. Inaba and Fukuda [14] investigated natural convection flow in an inclined rectangular cavity where the temperature of one wall was maintained at 0°C, while the temperature of the opposite hot wall was varied from 2 to 20°C. Lankford and Bejan [15] conducted experiments in a vertical enclosure where a constant heat flux boundary condition was imposed on the hot vertical wall, while the opposite wall was cooled. A combined experimental and analytical investigation of two-dimensional natural convection in a rectangular cavity was reported by Seki *et al.* [16]. The cold vertical wall was kept at 0°C, while the temperature of the hot wall was varied from 1 to 12°C. The predicted and measured temperature profiles had the same trends, but the agreement was not satisfactory.

Only two papers concerned with transient experiments in rectangular enclosures filled with water were identified during the literature search. Yewell *et al.* [17] investigated transient natural convection in low aspect ratio ($A = 0.0625$ and 0.112) enclosures at high Rayleigh numbers. They used water as a working fluid at temperatures between 15 and 35°C, where the density inversion does not occur. Ivey [18] conducted experiments in a square enclosure to study an initially isothermal cavity at temperature T_0, following the rapid change of the two vertical end walls to temperatures $T_0 \pm \Delta T$, respectively. He used water and a mixture of glycerol and water as the fluids. Once again, the density extremum in the fluid was not present.

This work has been motivated by the need to understand the development of the flow in the presence of the density inversion. Experiments were conducted with water that has its density extremum at 3.98°C. Four different series of experiments were carried out in a rectangular test cell with water having initial temperatures of 8, 12, 16 and 20°C. The fluid was initially stagnant and the temperature of one vertical wall was suddenly lowered to 0°C. A mathematical model was developed and the governing equations were solved numerically, and comparisons with test data are reported for all experimental conditions. The problem considered is not only of interest because of

NOMENCLATURE

A	aspect ratio, H/L
c	specific heat
g	gravitational acceleration
H	height of liquid level
k	thermal conductivity
L	length of cavity
P	dimensionless pressure, equation (11)
p	pressure
p^*	reduced pressure, $p+\rho_r gy$
Pr	Prandtl number, $\mu c/k$
R	density distribution parameter, equation (17)
Ra	Rayleigh number, equation (16)
T	temperature
t	time
U	dimensionless horizontal velocity, equation (11)
u	velocity component in the x-direction
V	dimensionless vertical velocity, equation (11)
v	velocity component in the y-direction
X	dimensionless horizontal coordinate, x/H
x	horizontal distance from cold wall
Y	dimensionless vertical coordinate, y/H
y	vertical coordinate.

Greek symbols

α	thermal diffusivity
θ	dimensionless temperature, $(T-T_c)/(T_h-T_c)$
μ	viscosity
ν	kinematic viscosity
ρ	density
τ	dimensionless time, equation (11).

Subscripts

c	cold
h	hot
m	maximum
r	reference.

its fundamental nature but is also relevant to freezing of water [19] and dilute water–salt solutions in a container when the temperature of one of the walls is suddenly lowered below the fusion temperature. In such a problem it is desirable to understand the flow structure, because it affects the local rate of solidification.

EXPERIMENTAL METHODS

The experiments were performed in a rectangular test cell having inside dimensions of 150 mm in height, 300 mm in length, and 75 mm in depth. Figure 1 shows schematically the experimental apparatus.

The right and left vertical walls in Fig. 1(a) consist of multipass copper heat exchangers that were plated with nickel and chrome to avoid corrosion. Each heat exchanger contained three loops through which the flow rate could be controlled independently. Five copper–constantan thermocouples (type-T) were placed very close to each heat-transfer surface, for continuous monitoring of its temperature. By adjusting the flow rate through the loops, it was possible to maintain the temperature of each heat exchanger uniform within $\pm 0.1^\circ$C of the desired temperature.

As it is shown in Fig. 1(a), the heat exchangers were connected through a valve system on two constant temperature baths. By an appropriate valve setting, the vertical end walls could be maintained at either the same or different temperatures. Ethyl alcohol was used as the working fluid in the constant temperature baths.

The horizontal bottom and top connecting walls as well as the front and back vertical walls were made of acrylic sheets in order to allow for flow visualization of the fluid motion inside the test cell. To minimize the heat gain from the ambient, the front and back walls were constructed from a pair of acrylic sheets with an air gap between them, and the entire test section was covered with 50 mm thick Styrofoam insulation. Two removable windows (shown in Fig. 1(b)) in the insulation (top and front walls) allowed for the illumination and visual observations.

Measurements of the temperature distributions inside the test cell were made also with (type-T) thermocouples. They were placed in a stainless steel tube having an o.d. of 0.9 mm. These probes were inserted through both horizontal walls where 42 holes (21 on each side) allowed their installation in several positions along the test cell. Typically, five probes were used in each wall (top and bottom), monitoring the temperature distributions in two different planes (see Fig. 1). A thermocouple rack was used to measure the temperature at the center plane of the test section. Figures 1(a) and (b) show schematically the configuration and the positions of the thermocouples. The thermocouple rack was made in order to minimize the heat conduction through its walls. With the same objective, the lower and upper planes of measurements were chosen close enough to the walls in order to avoid large variations in the temperature field where the thermocouples were exposed. The thermocouple output was recorded by a data logger system at preselected time intervals between two consecutive measurements.

Distilled water was used in all experiments, and the water was carefully siphoned into the test cell to avoid introduction of air. The test cell was not filled com-

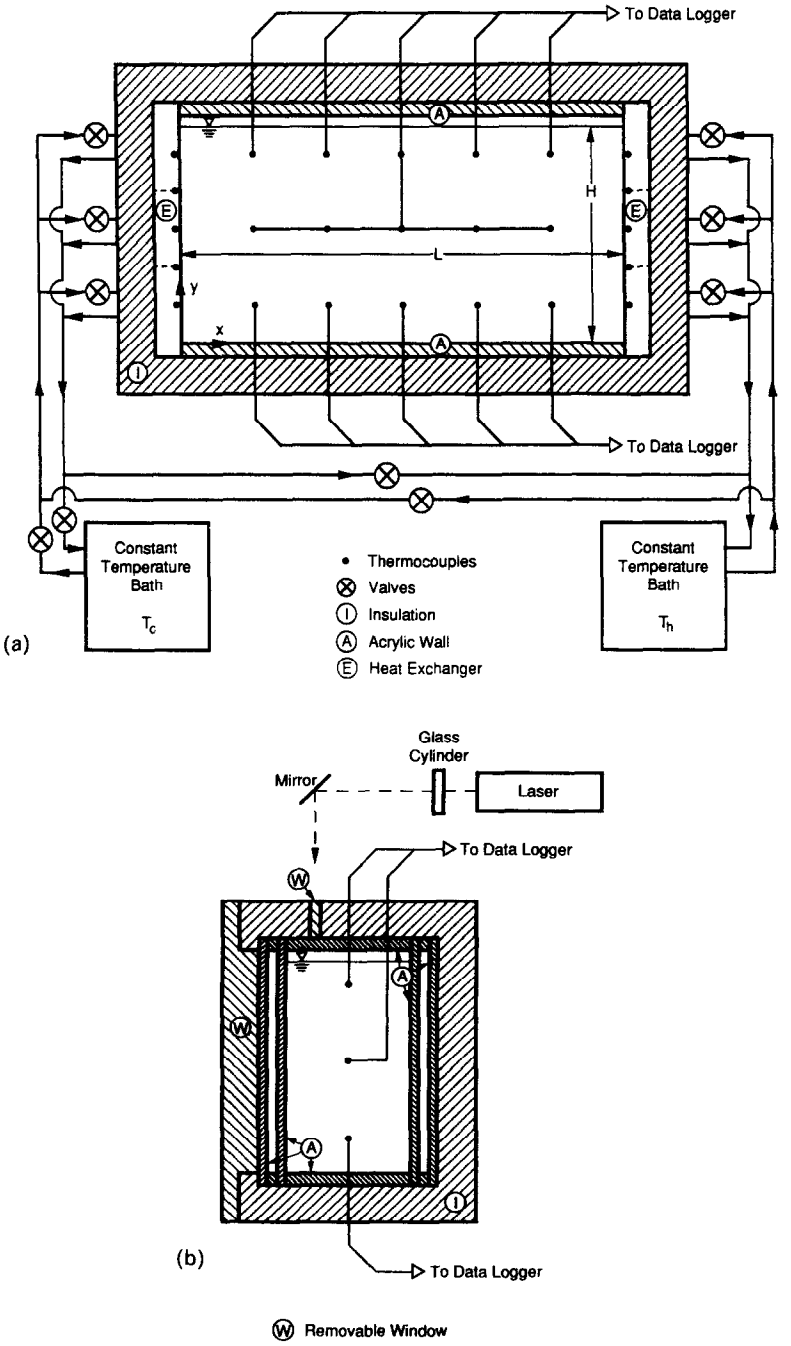

FIG. 1. Schematic diagram of the test cell: (a) front view; (b) end view.

pletely full of water, and a small (~ 3 mm) gap was left at the top in order to have a free surface (see Fig. 1) and to allow water to expand and/or to contract.

To start an experiment, both heat exchangers were coupled to the same bath and their surfaces were maintained at the desired temperature of the hot wall (T_h). Enough time was allowed until all the fluid in the test section reached a uniform temperature. The second constant temperature bath, with a preselected initial temperature (below 0°C), was connected to one of the heat exchangers. Typically, the desired temperature at the cold wall ($T_c = 0$°C) was reached between 1 and 2 min, depending on both the initial temperature of water in the test section and the bath temperature. The heat exchanger walls were kept at uniform temperatures by controlling individually the flows through each of the heat exchanger loops. Due to the transient nature of the experiments, the temperature settings of the constant temperature baths as well as the flow rates in the heat exchangers had to be frequently readjusted.

Previous experiments [19] were performed with the

cold wall temperature set below the freezing point. The solidification fronts did not show any significant spanwise nonuniformity due to the presence of the front and back walls of the test section, and therefore three-dimensional effects can be neglected.

To visualize the flow patterns, the water was seeded with a small amount of neutrally buoyant particles (Pliolite). A helium–neon laser was used as the illumination source. The laser beam was passed through a cylindrical glass rod to produce a sheet of laser light before passing it through the test cell wall. Figure 1(b) shows schematically the illumination system as well as the positions of the windows in the insulation. During the experiments the insulation covering the windows was kept in place (shown in Fig. 1(b)), except during the flow visualization periods. By controlling the quantity of particles and using a photographic camera, it was possible to obtain qualitative information about the seeded flow. Photographs of the flow patterns were taken using ASA 400 (T-MAX) film. The exposure time was about 100 s.

MATHEMATICAL MODEL AND NUMERICAL SOLUTION

We consider transient natural convective motion of water contained in a rectangular, two-dimensional cavity illustrated schematically in Fig. 1(a). A Cartesian coordinate system is located in the lower left-hand corner of the cavity. Initially ($t < 0$) the water is stagnant and at a uniform temperature (T_h) greater than 3.98°C. The vertical walls are maintained at $T = T_h$, and the top and bottom connecting walls are insulated. At time $t \geqslant 0$ a uniform temperature $T_c = 0$°C is imposed on the left vertical wall ($x = 0$), while the right vertical wall ($x = L$) is kept at $T = T_h$. The following simplifying assumptions are made in the analysis: (1) the flow is two-dimensional, laminar and incompressible, and (2) the thermophysical properties are independent of temperature, except for the density in the buoyancy force. These simplifications were made in order to reduce the computational effort and to enable comparison between predictions and data at earlier times during the transient.

The appropriate two-dimensional conservation of mass, momentum and energy equations governing the resulting transient fluid flow are, respectively

$$\frac{\partial u}{\partial x} + \frac{\partial v}{\partial y} = 0 \tag{1}$$

$$\rho_r\left(\frac{\partial u}{\partial t} + u\frac{\partial u}{\partial x} + v\frac{\partial u}{\partial y}\right) = -\frac{\partial p^*}{\partial x} + \mu\nabla^2 u \tag{2}$$

$$\rho_r\left(\frac{\partial u}{\partial t} + u\frac{\partial u}{\partial x} + v\frac{\partial v}{\partial y}\right) = -\frac{\partial p^*}{\partial y} + \mu\nabla^2 v - \rho g \tag{3}$$

$$\rho_r c\left(\frac{\partial T}{\partial t} + u\frac{\partial T}{\partial x} + v\frac{\partial T}{\partial y}\right) = k\nabla^2 T. \tag{4}$$

The initial and boundary conditions are

$$u = v = 0 \quad \text{and} \quad T = T_h \quad \text{for} \quad t < 0 \tag{5}$$

and

$$T = T_c \quad \text{at} \quad x = 0 \quad \text{and} \quad 0 \leqslant y \leqslant H \tag{6}$$

$$T = T_h \quad \text{at} \quad x = L \quad \text{and} \quad 0 \leqslant y \leqslant H \tag{7}$$

$$\frac{\partial T}{\partial y} = 0 \quad \text{at} \quad y = 0 \quad \text{and} \quad H \quad \text{for} \quad 0 \leqslant x \leqslant L. \tag{8}$$

There is no slip at the walls, and at the free surface the boundary conditions for the velocity are

$$\frac{\partial u}{\partial y} = v = 0 \quad \text{at} \quad y = H \quad \text{for} \quad 0 \leqslant x \leqslant L. \tag{9}$$

The thermocapillary effects have been neglected. According to the criteria suggested by Ostrach [20], the parameter which determines the relative importance of buoyancy to surface tension gradients for boundary layer flows is $Gr_H(A/Re_{\sigma,H})^{5/3}$, where Gr_H is the Grashof number and $Re_{\sigma,H}$ the surface tension Reynolds number. For the geometry, thermal conditions imposed and water as the test fluid, estimates have revealed that neglect of thermocapillary effects is justified.

In equation (3), ρg is the buoyancy force, with ρ being the local density corresponding to the local temperature. For fluids having a linear density–temperature relationship, the usual Boussinesq approximation can be used for the buoyancy term. However, water has a non-linear density–temperature relationship that attains its maximum at $T = 3.98$°C. Several authors have proposed different correlations for the density of water as a function of temperature. In this study, the approximation suggested by Gebhart and Mollendorf [21, 22] is used

$$\rho = \rho_m(1 - \omega|T - T_m|^q) \tag{10}$$

where ρ_m is the maximum density ($\rho_m = 999.972$ kg m^{-3}), $\omega = 9.297173 \times 10^{6}$°C^{-q}, $T_m = 4.0293$°C and $q = 1.894816$.

To reduce the number of parameters for the numerical solutions, dimensionless variables and groups are introduced as

$$X = \frac{x}{H}, \quad Y = \frac{y}{H}, \quad U = \frac{u}{\alpha/H}, \quad V = \frac{v}{\alpha/H}$$

$$\theta = \frac{T - T_c}{T_h - T_c}, \quad \tau = \frac{t}{H^2/\nu}, \quad P = \frac{p^*}{\rho_r(\alpha/H)^2 Pr}. \tag{11}$$

With the aforementioned variables, the conservation equations in dimensionless form can be written as

$$\frac{\partial U}{\partial X} + \frac{\partial V}{\partial Y} = 0 \tag{12}$$

$$\frac{\partial U}{\partial \tau} + \frac{1}{Pr}\left(U\frac{\partial U}{\partial X} + V\frac{\partial U}{\partial Y}\right) = -\frac{\partial P}{\partial X} + \frac{\partial^2 U}{\partial X^2} + \frac{\partial^2 U}{\partial Y^2} \tag{13}$$

$$\frac{\partial V}{\partial \tau}+\frac{1}{Pr}\left(U\frac{\partial V}{\partial X}+V\frac{\partial V}{\partial Y}\right)=-\frac{\partial P}{\partial Y}$$

$$+Ra[(\theta-R)^q-(1-R)^q]+\frac{\partial^2 V}{\partial X^2}+\frac{\partial^2 V}{\partial Y^2} \quad (14)$$

$$Pr\frac{\partial \theta}{\partial \tau}+U\frac{\partial \theta}{\partial X}+V\frac{\partial \theta}{\partial Y}=\nabla^2\theta \quad (15)$$

where

$$Ra=\frac{\rho_m g\omega H^3(T_h-T_c)^q}{\rho_r \nu\alpha} \quad (16)$$

is the modified Rayleigh number and

$$R=\frac{T_m-T_c}{T_h-T_c} \quad (17)$$

is the density distribution parameter. If $0<R<1$ ($T_c<T_m<T_h$) the maximum density will occur in the water. The modified Rayleigh number Ra for water near its density maximum given by equation (16) is defined differently than for ordinary fluids. Since $q=1.895$, the modified Rayleigh number is not proportional to (T_h-T_c) but to $(T_h-T_c)^{1.895}$. In addition, the density distribution parameter R defines the position of the maximum temperature relative to the temperature difference across the cavity.

The model equations are solved numerically using a control volume based finite-difference formulation [23]. A non-uniform mesh of $M\times N$ nodes is employed, and the SIMPLER algorithm [23] is used to solve iteratively the system of finite-difference equations. Determination of an acceptable mesh size is of prime importance since the greater computational accuracy obtainable with larger values of M and N must be balanced against computer time requirements.

Grid sensitivity studies were conducted starting with a uniform grid of $M=N=50$ and time step of $\Delta\tau=7.7\times10^{-5}$ ($\Delta t=1$ s). A large number of meshes and time steps were tested for typical situations. The predicted streamlines and isotherms were analyzed in order to determine the mesh for which results are grid independent and to define the conditions for adoption in the final simulations. The mesh and time steps were chosen as a compromise between computer cost and accuracy. The results reported in the paper were obtained with a non-uniform grid of 98×47 nodal points. The non-uniform grid provided a higher concentration of nodes near the walls of the enclosure where the velocity and thermal gradients need to be accurately resolved. Two different time steps of $\Delta\tau\simeq8\times10^{-4}$ ($\Delta t=1$ s) and $\Delta\tau\simeq2\times10^{-4}$ ($\Delta t=3$ s) were used in the simulations. The smaller time increment was used from $\tau=0$ until $\tau\simeq0.013$ ($t=5$ min) and the larger one from $\tau\gtrsim0.013$ until the termination of the calculations.

RESULTS AND DISCUSSION

Experimental conditions

Four different series of experiments were performed by covering a wide range of initial and hot wall temperatures T_h (8, 12, 16 and 20°C). The principal dimensionless groups (Pr, Ra and R) are summarized in Table 1.

In all cases, enough time was allowed until the desired initial temperature was reached between ±0.1°C. In the beginning of each experiment, typically 1 or 2 min were required to achieve the desired temperature at the cold wall. Both the cold and the hot wall temperatures were maintained constant within ±0.1°C of the desired values by controlling independently the flows through each of the three loops in the heat exchangers.

All experiments were repeated at least twice: once for data acquisition and once for flow visualization purposes when part of the insulation was removed (one window for illumination and another to allow for visual observations). In all cases, the perturbation of the system due to insulation removal was very small, and the temperature field inside the test cell was not significantly affected. Freezing of the water was not observed in any of the experiments.

With the same initial and boundary conditions of the experimental cases, four numerical simulations were performed. Due to the excessive computer processing time requirements, typically the first 30 min ($\tau=0.14$) of each experiment were simulated. The only exception was experiment 4 ($T_h=20$°C) when $\tau=0.21$ ($t=45$ min) was simulated. For all experiments the velocity and temperature fields were predicted and at selected times streamlines and isotherms are plotted. From the results obtained it is possible to analyze the development of the flow field as well as the influences of the density extremum. For the isotherms, the left vertical wall ($X=0$) corresponds to $\theta=0$ ($T=T_c$) while the right one ($X=1$) corresponds to $\theta=1$ ($T=T_h$).

Experiment No. 1

The results can be presented in a more meaningful way in the form of transient streamlines and isotherms. Streamlines give an immediate picture of the flow structure in the cavity, and the isotherms are important as they indicate the density distribution inside the flow field. Specifically, the 4°C isotherm, when superimposed on the streamline pattern, will give the location of the maximum density. This is

Table 1. Summary of experimental conditions

Experiment No.	T_h (°C)	Pr	Ra (1×10^{-8})	R
1	8	11.82	0.66	0.50
2	12	11.05	1.49	0.34
3	16	10.33	2.71	0.25
4	20	9.67	4.36	0.20

demonstrated by comparing the streamlines and isotherms presented in Figs. 2 and 3, respectively, at the corresponding times. In this particular experiment, $\theta \simeq 0.5$ corresponds to the density maximum. The numerical results obtained for experiment 1 ($T_h = 8°C$) are discussed first in some detail. In this experiment the density inversion occurs at $\theta \cong 0.5$ ($T \cong 4°C$). This isotherm divides the test cell into two parts. In order to better illustrate what happens, the streamlines obtained for the same simulation are presented in Fig. 3.

At the very beginning of the cooling process, heat transfer is by conduction. It is clearly evident from Figs. 2(a) and 3(a) that at $\tau = 0.023$ ($t = 5$ min) a boundary layer type motion is set up near the cold wall and convection is initiated. The flow gradually fills the entire cavity at later times (Fig. 3(c)). A large counterclockwise rotating circulation can be seen, and

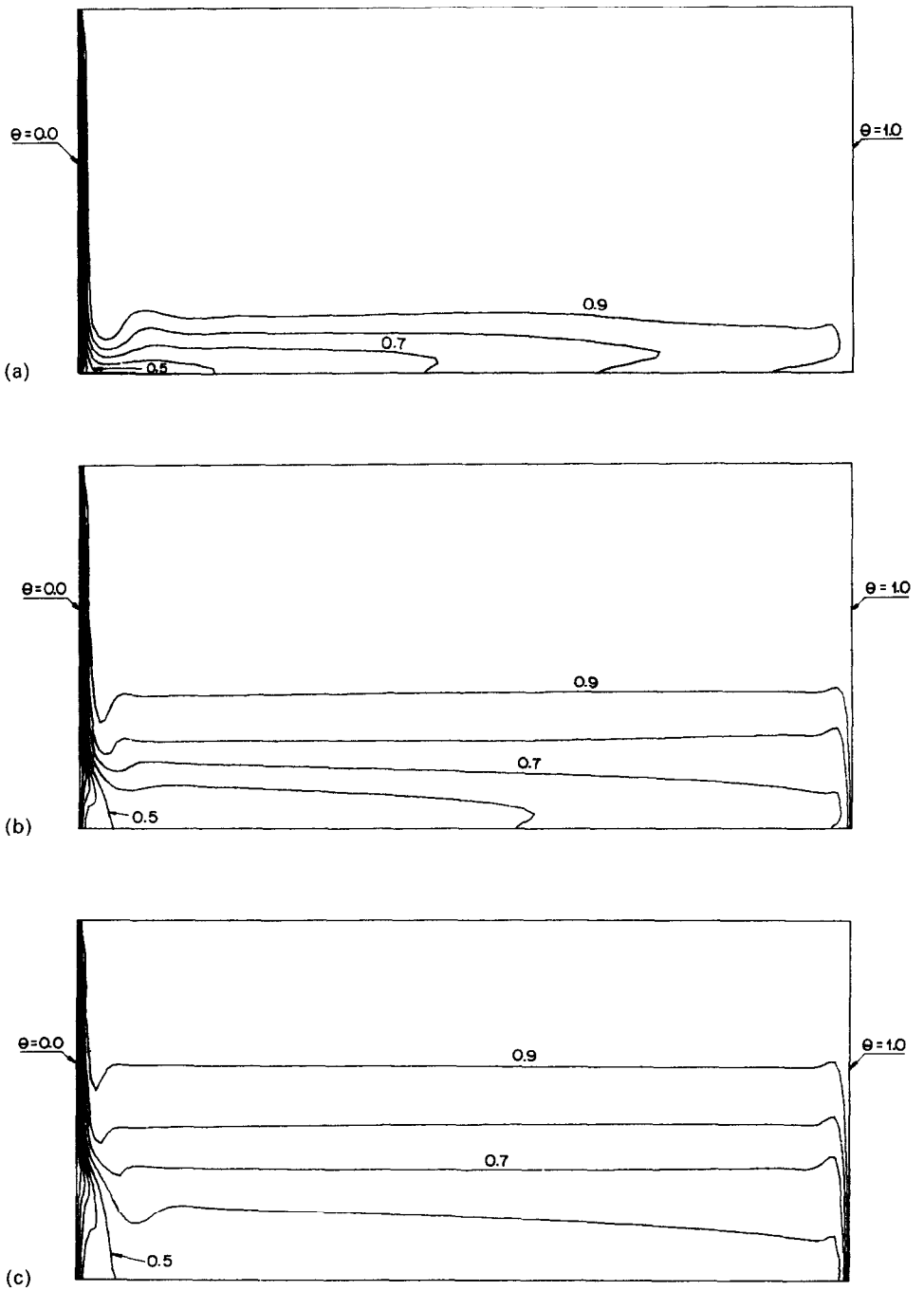

FIG. 2. Predicted isotherms for Experiment 1 with $T_h = 8°C$: (a) $\tau = 0.023$ ($t = 5$ min); (b) $\tau = 0.0695$ ($t = 15$ min); (c) $\tau = 0.139$ ($t = 30$ min).

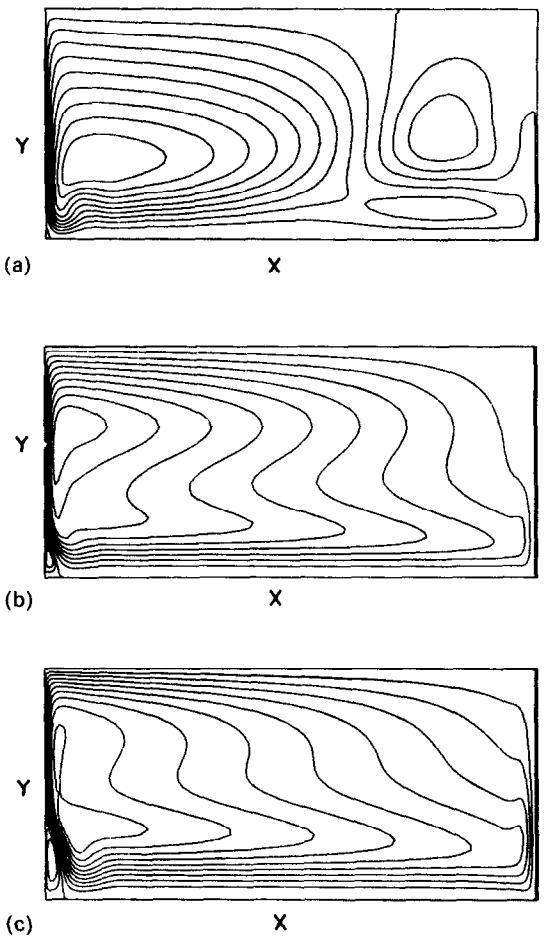

FIG. 3. Predicted streamlines for $T_h = 8°C$: (a) $\tau = 0.023$ ($t = 5$ min), $\psi_{max} = 38.6$, $\psi_{min} = 141.1$; (b) $\tau = 0.0695$ ($t = 15$ min), $\psi_{max} = 6.4$, $\psi_{min} = -70.6$; (c) $\tau = 0.139$ ($t = 30$ min), $\psi_{max} = 11.1$, $\psi_{min} = 48.4$.

it embraces almost the entire test section. The hot fluid ($T > 4°C$) flows down along the cold wall while it is being cooled on the left side of the circulation, and the water flows upward while it is heated by the right wall. On the other hand, the opposite occurs on the left side of the $\theta \simeq 0.5$ isotherm, where the fluid descends when it is heated and flows up when it is cooled. In this case, a small clockwise circulation grows in the lower left-hand corner of the cavity with time. These two opposite circulations are caused by the density inversion, and they are separated by the isotherm $T = T_m$ (compare the corresponding cases in Figs. 2 and 3).

At early times, $\tau < 2.3 \times 10^{-2}$ ($t < 5$ min), the numerical results reveal that the flow is initially dominated by the vertical motion associated with the downward flow over the cold (left) wall. The fluid in this region tends to sink while the lighter fluid in the right-hand side of the test cell is forced upward by continuity. After $\tau = 2.3 \times 10^{-2}$, the upward motion associated with the flow over the hot (right) wall becomes significant (Fig. 3(a)). At this time the cell that is expected in the lower left-hand corner of the cavity ($T_c < T < T_m$) is insignificant. This circulation, however, appears clearly in Figs. 3(b) and (c). The symmetrical flow that would be expected purely from steady state considerations for $T_c = 0°C$, $T_h = 8°C$ and $R \cong 0.5$ [5, 7, 11, 14, 15] in a completely filled cavity does not occur in the present experiments. The references cited report results for cavities completely filled with a fluid (i.e. no slip condition at the upper wall of the cavity). The free surface condition of this study imposes $\partial u/\partial y = 0$ at $y = H$. This requirement accepts $u \neq 0$. Unsymmetric flow is predicted, and this finding is in agreement with flow visualization results. For $\tau = 0.14$ (Fig. 3(c)), the flow is not yet at steady state, and the computations were terminated owing to the excessive computer processing time requirements. The results show that the flow is clearly not symmetrical about the vertical centerline of the cavity during the transient.

Figure 4 shows the photographs obtained at $\tau = 0.007$ and 0.14 (15 and 30 min) after the start of the first experiment. A comparison of Figs. 3(b) and 4(a) as well as 3(c) and 4(b) reveals good agreement. Details of the flow patterns are very similar when the predicted streamlines, in the large circulation cell, are compared with the same region in the photographs. The circulations in the lower left-hand corner of the cavity appear smaller in the predictions than in the experiments. Heat conduction through the bottom connecting wall can cause the $\theta = 0.5$ isotherm to move to the right, thereby increasing the size of the circulation cell. This appears to be the most important reason for the difference. The second reason is associated with the fact that in the mathematical model the thermophysical properties are assumed to be constant. The temperature has an appreciable influence on the thermophysical properties, particularly when the viscosity is considered [5]. A third reason for the discrepancy is that the numerical simulation assumes the cold wall temperature to change instantaneously at $\tau = 0$, and in the experiment it takes about 1–2 min for the surface temperature to reach a constant value. This discrepancy caused by the modeling idealization is expected to diminish with time, but it was not completely eliminated.

Careful comparison of the calculated (Fig. 3) and observed (Fig. 4) flow patterns reveals good agreement and that the experimental flow patterns at $\tau = 0.14$ ($t = 30$ min) (not yet at full steady state) are not symmetrical about the vertical line at the center of the cavity. The results suggest that either the initial water temperature, the imposed boundary conditions and/or the aspect ratio of the cavity combine to make the flow unsymmetrical. For the experimental conditions, the symmetrical flow pattern expected on the basis of previous studies for different geometries and boundary conditions did not develop during the course of the experiment. This is supportive of the experimental findings reported by Inaba and Fukuda [14] and Seki *et al.* [16] for a square cavity with

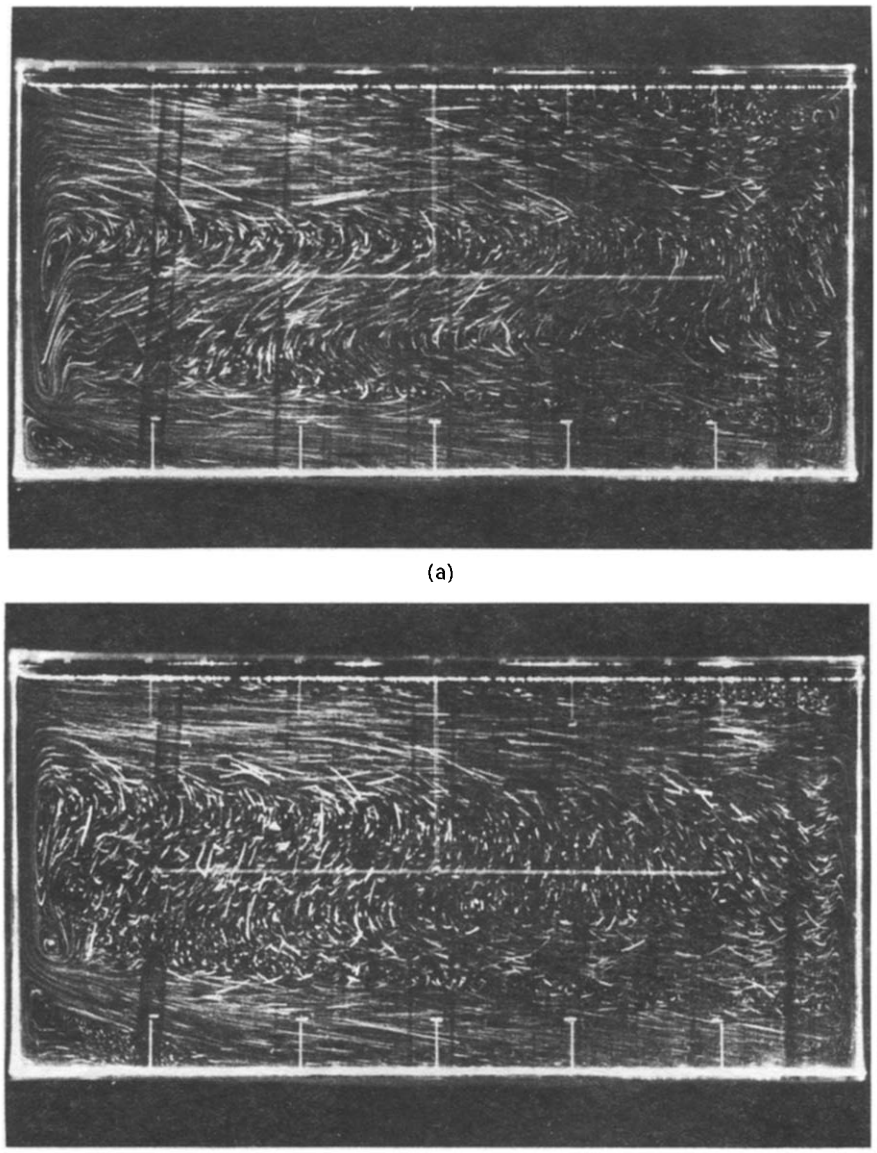

(a)

(b)

FIG. 4. Photographs of flow pattern for $T_h = 8°C$: (a) $\tau = 0.0695$ ($t = 15$ min); (b) $\tau = 0.139$ ($t = 30$ min).

the flow generated by a step change in the hot wall temperature to 8°C. They needed about 6–15 h to obtain steady-state conditions. The steady-state flow patterns they observed in a cavity having an aspect ratio of unity were not truly symmetrical, but were not as much distorted (particularly the $\theta = 0.5$ isotherm) as those observed in the present work. Part of the difference is attributed to the different aspect ratios, boundary as well as initial conditions, and conjugate effects in the two studies.

The comparisons between the predicted and measured temperature distributions for Experiment 1 are presented in Fig. 5. The comparisons are made at three different vertical positions and different times. It is evident that, in general, the experimental results agree well with the predictions. It is interesting to note that the thermocouples inserted through the top connecting wall show a temperature equal to or slightly higher than the predicted temperature, while the other thermocouples inserted through the bottom wall reveal the opposite trend. This difference is due to heat conduction along the thermocouple probes. The largest discrepancy at each time is in the thermocouple closest to the cool wall located near the bottom of the cavity ($Y = 0.119$). The maximum difference is only about 2.0°C out of the total temperature difference of 8°C across the entire cavity for this particular experiment. It is in this region that the temperature gradient is largest along the probes, increasing the fin effect (see Fig. 2). The simplifying assumptions adopted in the mathematical model such as temperature independent thermophysical properties, two-dimensional flow and heat transfer, absence of conjugate effects, and numerical approximations should also be considered as additional reasons responsible for the discrepancies.

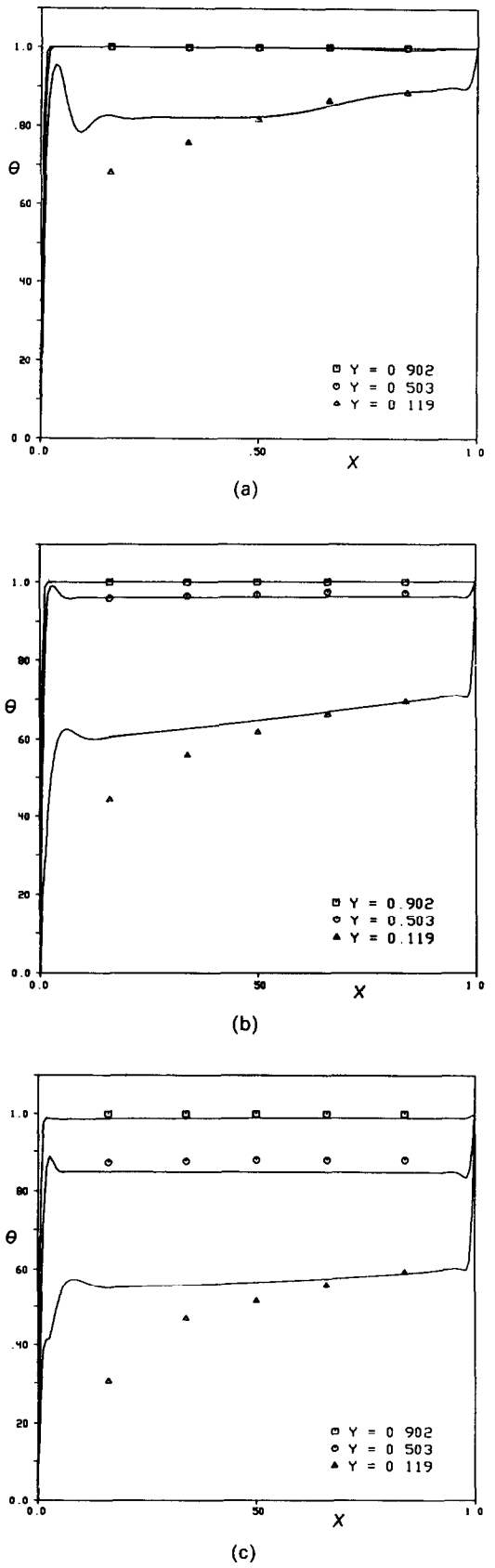

FIG. 5. Comparison between predicted and measured temperatures with $T_h = 8°C$: (a) $\tau = 0.023$ ($t = 5$ min); (b) $\tau = 0.0695$ ($t = 15$ min); (c) $\tau = 0.139$ ($t = 30$ min).

Other experiments

The same procedure adopted for Experiment 1 was repeated for the other experiments. Figures 6–8 show the comparisons between predicted and observed flow patterns for Experiments 2–4, respectively. Good agreement is also noted in all these cases.

Figure 6(a) shows the comparison of the predicted and visualized flows for $\tau = 0.065$ ($t = 15$ min) and $T_h = 12°C$. It is clear that the circulation in the lower left-hand corner is very small and is barely identifiable in the figure. For $\tau = 0.13$ ($t = 30$ min) (see Fig. 6(b)) this circulation appears bigger in both the predicted and visualized streamlines. It is interesting to note that for Experiment 1 at $\tau = 0.07$ ($t = 15$ min) (Figs. 3(b) and 4(a)) the rotating edge in the left corner is evident. Inspection of the upper right-hand corner in Fig. 6 reveals that the vertical upward flow over the hot wall becomes stronger with time.

For the experiment with $T_h = 16°C$, Fig. 7 shows exactly the same flow patterns as those illustrated in Fig. 6 for Experiment 2. Here, the small circulation that appears in the left part of the cavity is weaker due to the higher hot wall temperature.

The simulation of Experiment 4 was extended to $t = 45$ min ($\tau = 0.174$) in order to examine the development of the small circulations that was not evident up to $t = 30$ min ($\tau = 0.116$). Figure 8(b) shows that this rotating cell is very small for $t = 45$ min ($\tau = 0.174$) while for $t = 22$ min ($\tau = 0.085$) (Fig. 8(a)) it is not evident at all, and the large counterclockwise rotating cell embraces the entire test section. As it is indicated in Table 1, Experiment 4 had the minimum R that justifies the smaller circulations in the left-hand corner (the region where $T < T_m$ is relatively small).

The comparisons between the measured and predicted temperatures for Experiments 2–4 are presented in Figs. 9–11. The agreement is considered good, and the same type of trends are evident as for Experiment 1.

Examination of Figs. 6–11 reveals that the influence of the density inversion of water increases with the decrease in the initial temperature. This was expected and can be explained by the fact that the 4°C isotherm moves further to the right from the left, cold wall for experiments which have a lower T_h (>4°C). This can be associated with the density distribution parameter R that increases with the decreasing T_h. Direct comparisons with published results are not possible because of the geometries and/or boundary conditions used.

Another point to be considered when comparing the measured and predicted results is the grid size. A non-uniform grid was used in the simulations in order to have a fine grid close to the walls, where larger velocity and temperature gradients are expected. This type of grid improved the resolution and yielded more accurate results than the ones which could be obtained with a uniform grid. The number of nodes was chosen as a compromise between computer cost and

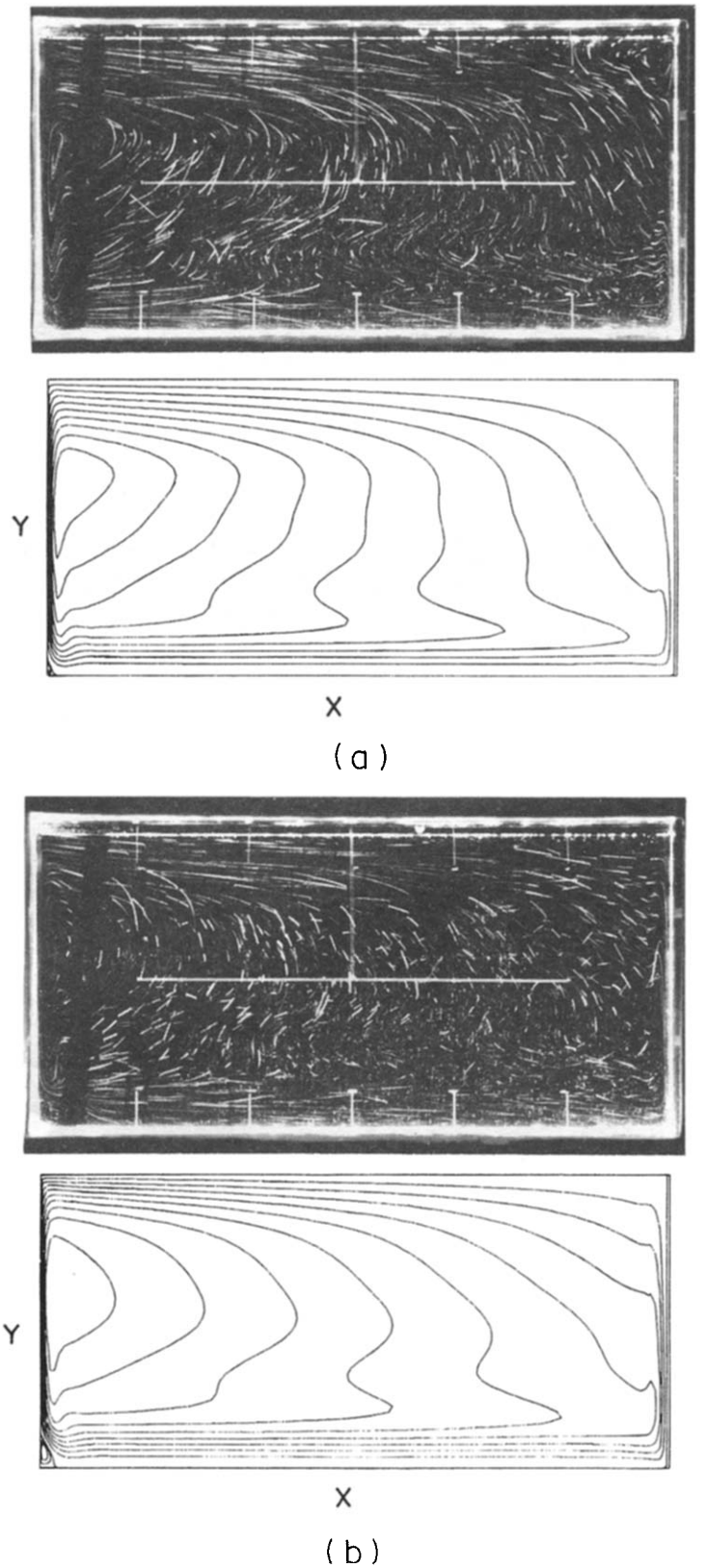

FIG. 6. Predicted streamlines and photographs for Experiment 2 with $T_h = 12°C$: (a) $\tau = 0.065$ ($t = 15$ min), $\psi_{max} = 1.3$, $\psi_{min} = 83.4$; (b) $\tau = 0.13$ ($t = 30$ min), $\psi_{max} = 3.8$, $\psi_{min} = 57.7$.

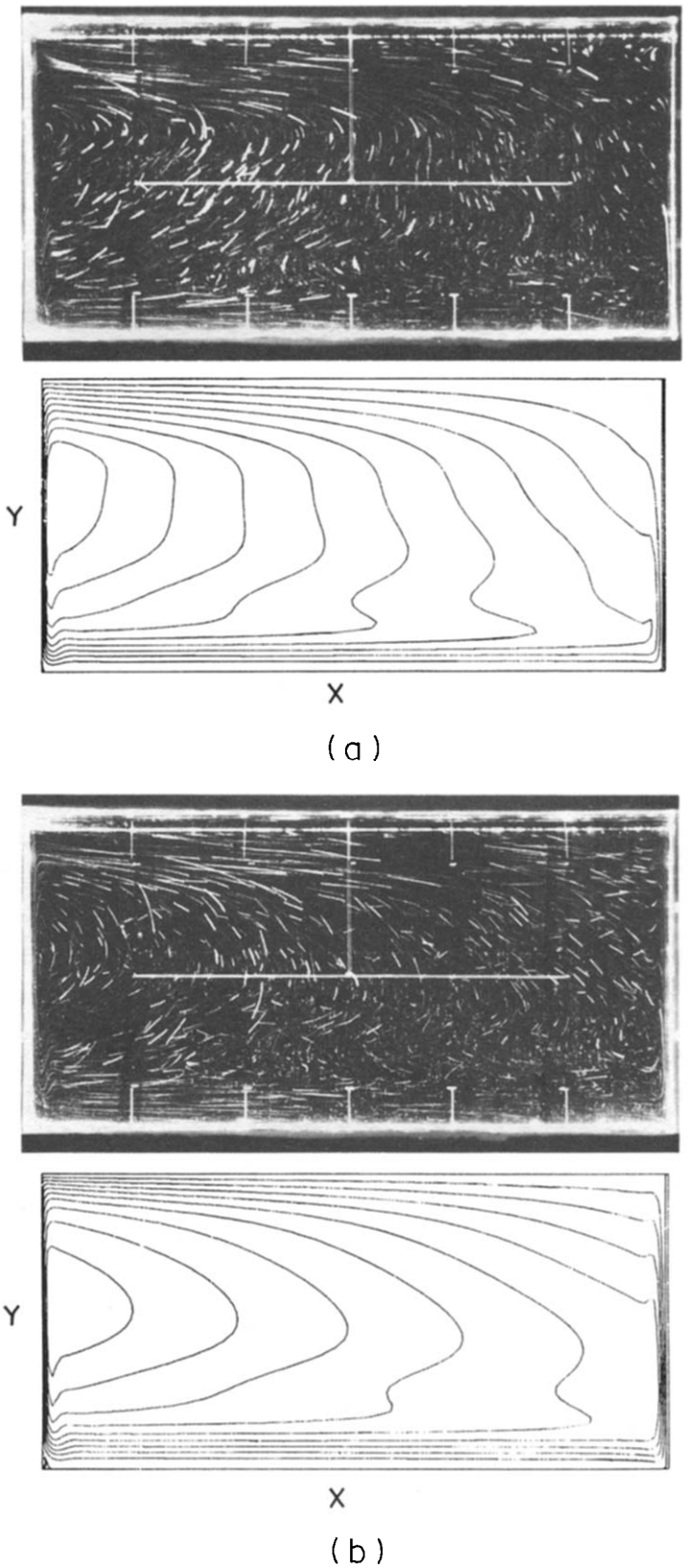

FIG. 7. Predicted streamlines and photographs for Experiment 3 with $T_h = 16°C$: (a) $\tau = 0.0615$ ($t = 15$ min), $\psi_{max} = 0.5$, $\psi_{min} = -86.6$; (b) $\tau = 0.123$ ($t = 30$ min), $\psi_{max} = 1.3$, $\psi_{min} = -64.7$.

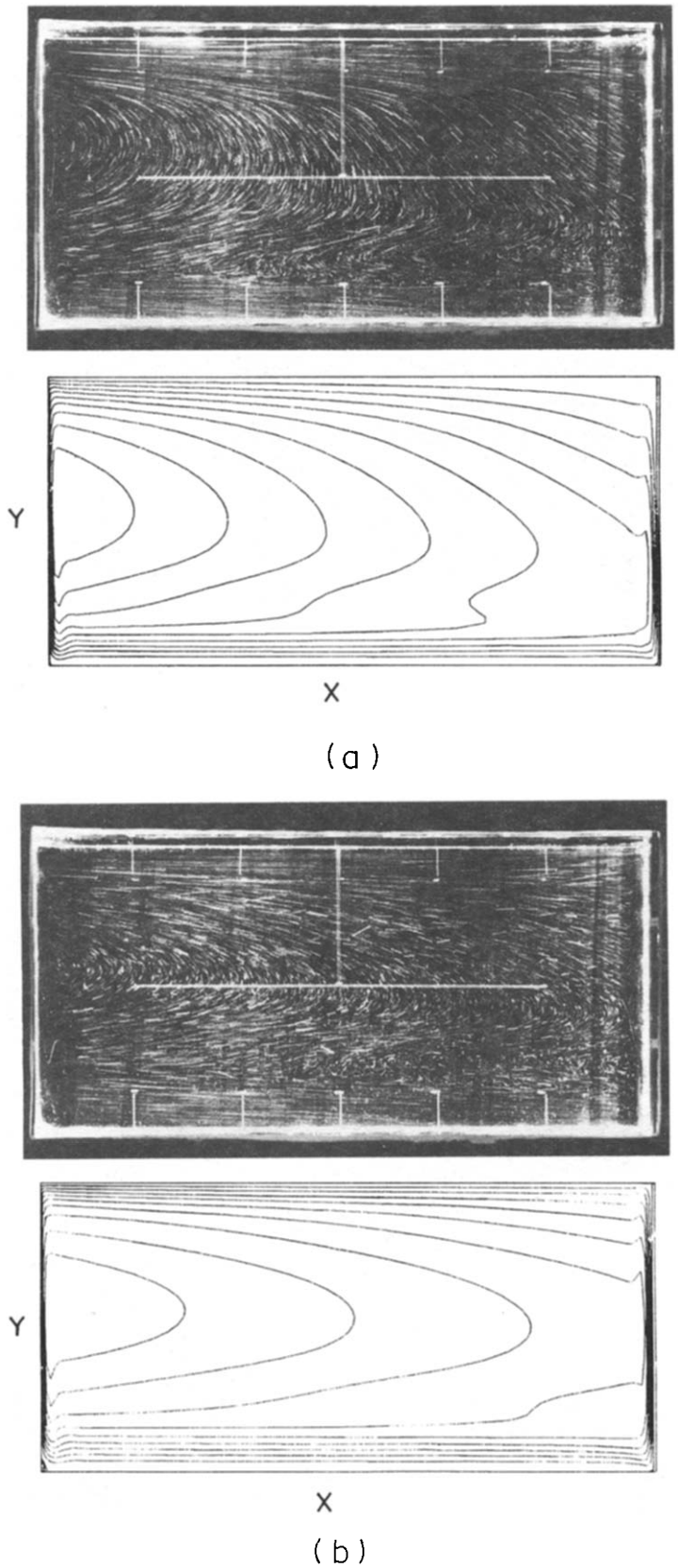

FIG. 8. Predicted streamlines and photographs for Experiment 4 with $T_h = 20°C$: (a) $\tau = 0.085$ ($t = 22$ min), $\psi_{max} = 0.4$, $\psi_{min} = -83.0$; (b) $\tau = 0.174$ ($t = 45$ min), $\psi_{max} = 1.1$, $\psi_{min} = -67.3$.

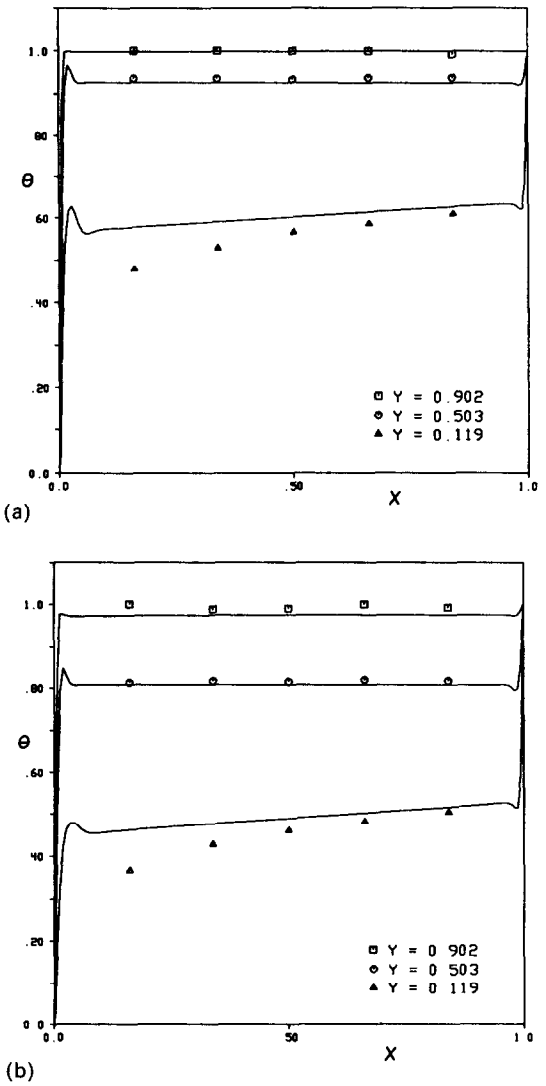

FIG. 9. Comparisons between predicted and measured temperatures for Experiment 2 with $T_h = 12°C$: (a) $\tau = 0.065$ ($t = 15$ min); (b) $\tau = 0.13$ ($t = 30$ min).

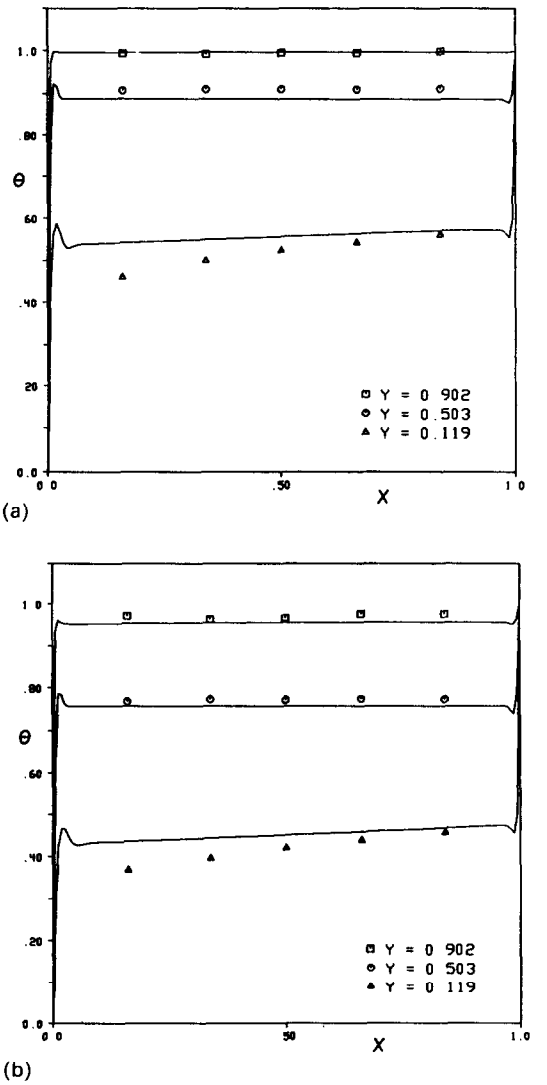

FIG. 10. Comparisons between predicted and measured temperatures for Experiment 3 with $T_h = 16°C$: (a) $\tau = 0.0605$ ($t = 15$ min); (b) $\tau = 0.123$ ($t = 30$ min).

accuracy. A larger number of nodes would have been desirable, but the calculations were extremely time consuming. Finally, the flow and temperature fields in the cavity are truly three-dimensional and their idealization using a two-dimensional model is inadequate to resolve all of the structural details of the fields.

CONCLUSIONS

The transient behavior of thermally driven convection in a partially filled (with a free surface) rectangular cavity containing water near the density inversion is studied both experimentally and numerically. The results are presented for four different experiments where the initial temperature is varied from 8 to 20°C in order to examine its influence on the effect of the density extremum on the flow structure and temperature distribution. The results obtained in the study can be summarized as follows:

(1) The density inversion of water has an important effect on natural convection flow and heat transfer.

(2) In all experiments performed, two counter-rotating eddies arose in the test section which were caused by the density inversion.

(3) The predicted and measured temperature distributions as well as flow structures are in good agreement.

(4) The results obtained indicate that for the initial and boundary ($T_h = 0$ and 8°C) conditions considered nearly symmetrical flow, with two oppositely rotating vortices expected at steady-state for a no-slip boundary condition at the top of the cavity, does not develop during the course of the experiment when a no-shear boundary condition is imposed.

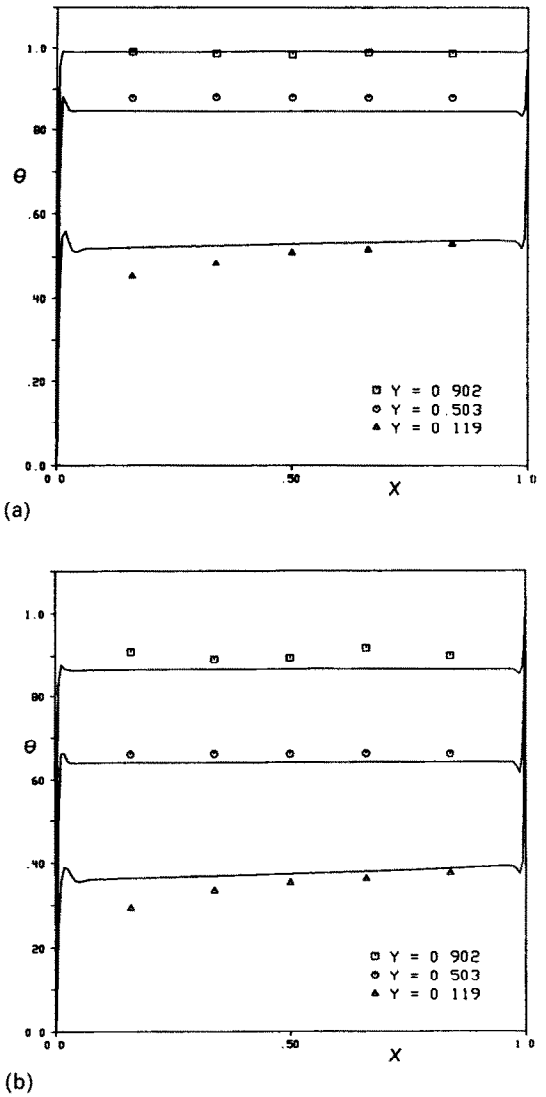

FIG. 11. Comparisons between predicted and measured temperatures for Experiment 4 with $T_h = 20°C$: (a) $\tau = 0.058$ ($t = 15$ min); (b) $\tau = 0.174$ ($t = 45$ min).

Acknowledgements—This work was done when one of the authors (S.L.B.) held a visiting appointment at Purdue University. He would like to express his appreciation to the Brazilian Government for supporting his sabbatical leave during the 1988–89 academic year.

REFERENCES

1. D. S. Lin and M. W. Nansteel, Natural convection in a vertical annulus containing water near the density maximum, *J. Heat Transfer* **109,** 899–905 (1987).
2. C. J. Ho and Y. H. Lin, Natural convection heat transfer of cold water within an eccentric horizontal cylindrical annulus, *J. Heat Transfer* **110,** 894–900 (1988).
3. B. Gebhart, M. S. Bendel and H. Shaukatullah, Buoyancy induced flows adjacent to horizontal surfaces in water near its density extremum, *Int. J. Heat Mass Transfer* **22,** 137–149 (1979).
4. J. C. Mollendorf and K. H. Jahn, Onset of convection in a horizontal layer of cold water, *J. Heat Transfer* **105,** 460–464 (1983).
5. A. Watson, The effect of the inversion temperature on the convection of water in an enclosed rectangular cavity, *Q. J. Mech. Appl. Math.* **25,** 423–446 (1972).
6. D. S. Lin and M. W. Nansteel, Natural convection heat transfer in a square enclosure containing water near its density maximum, *Int. J. Heat Mass Transfer* **30,** 2319–2328 (1987).
7. M. W. Nansteel, K. Medjani and D. S. Lin, Natural convection of water near its density maximum in a rectangular enclosure: low Rayleigh number calculations, *Physics Fluids* **30,** 312–317 (1987).
8. R. E. Forbes and J. W. Cooper, Natural convection in a horizontal layer of water cooled from above to near freezing, *J. Heat Transfer* **97,** 47–53 (1975).
9. L. Robillard and P. Vasseur, Convective response of a mass of water near 4°C to a constant cooling rate applied on its boundaries, *J. Fluid Mech.* **118,** 123–141 (1982).
10. L. Robillard and P. Vasseur, Transient natural convection heat transfer of water with maximum density effect and supercooling, *J. Heat Transfer* **103,** 528–534 (1981).
11. L. Robillard and P. Vasseur, Effet du maximum de densité sur la convection libre de l'eau dans une cavité fermée, *Can. J. Civil Engng* **6**(4), 481–493 (1979).
12. P. Vasseur and L. Robillard, Transient natural convection heat transfer in a mass of water cooled through 4°C, *Int. J. Heat Mass Transfer* **23,** 1195–1205 (1980).
13. K. C. Cheng, H. Inaba and R. R. Gilpin, Effects of natural convection on ice formation around an isothermally cooled horizontal cylinder, *J. Heat Transfer* **100,** 931–937 (1988).
14. H. Inaba and T. Fukuda, An experimental study of natural convection in an inclined rectangular cavity filled with water at its density extremum, *J. Heat Transfer* **106,** 109–115 (1984).
15. K. E. Lankford and A. Bejan, Natural convection in a vertical enclosure filled with water near 4°C, *J. Heat Transfer* **108,** 755–763 (1986).
16. N. Seki, S. Fukusako and H. Inaba, Free convective heat transfer with density inversion in a confined rectangular vessel, *Wärme- und Stoffübert.* **11,** 145–156 (1978).
17. R. Yewell, D. Poulikakos and A. Bejan, Transient natural convection experiments in shallow enclosures, *J. Heat Transfer* **104,** 533–538 (1982).
18. G. N. Ivey, Experiments on transient natural convection in a cavity, *J. Fluid Mech.* **144,** 389–410 (1984).
19. S. L. Braga and R. Viskanta, Effect of water density extremum on the solidification process, *Experimental Heat Transfer, Fluid Mechanics, and Thermodynamics 1991* (Edited by J. F. Keffer, R. K. Shah and E. N. Ganić), pp. 1185–1192. Elsevier, New York (1991).
20. S. Ostrach, Fluid mechanics in crystal growth—The 1982 Freeman Scholar Lecture, *J. Fluids Engng* **105,** 5–20 (1983).
21. B. Gebhart and J. Mollendorf, A new density relation for pure and saline water, *Deep Sea Res.* **24,** 831–848 (1977).
22. B. Gebhart and J. Mollendorf, Buoyancy-induced flows in water under conditions in which density extrema may arise, *J. Fluid Mech.* **89,** 673–707 (1978).
23. S. V. Patankar, *Numerical Heat Transfer and Fluid Flow.* McGraw-Hill, New York (1980).

CONVECTION NATURELLE VARIABLE DANS L'EAU, PRES DE SON MAXIMUM DE DENSITE, DANS UNE CAVITE RECTANGULAIRE

Résumé—On rapporte une étude expérimentale et théorique de la convection thermique naturelle variable dans l'eau près de son maximum de densité, dans une cavité rectangulaire. On impose des températures différentes sur les parois verticales opposées et les effets de l'inversion de densité au voisinage de 4°C sont étudiés. Initialement le fluide dans la cellule d'essai est à température uniforme et la température d'une des parois verticales froides est abaissée brusquement et maintenue à 0°C. La paroi chaude est maintenue à une température constante pendant l'expérience et égale à la température initiale de l'eau qui varie de 8 à 20°C. Des solutions des équations sont obtenues numériquement pour toutes les expériences réalisées. On présente des photographies de visualisation d'écoulement et des prédictions de configuration d'écoulement, ainsi que des comparaisons entre températures mesurées et calculées. On montre que l'inversion de densité a une grande influence sur la convection naturelle dans la cavité et que la structure de l'écoulement ne peut pas être prédite en utilisant les modèles classiques de convection naturelle qui emploient l'approximation de Boussinesq.

INSTATIONÄRE NATÜRLICHE KONVEKTION VON WASSER NAHE SEINEM DICHTEEXTREMUM IN EINEM RECHTECKIGEN HOHLRAUM

Zusammenfassung—Es werden experimentelle und theoretische Untersuchungen zum Wärmeübergang bei instationärer natürlicher Konvektion von Wasser nahe seinem Dichteextremum in einem rechteckigen Hohlraum vorgestellt. Den gegenüberliegenden senkrechten Wänden werden verschiedene Temperaturen aufgeprägt. Es wird der Einfluß der Dichteinversion untersucht. Zu Beginn besitzen das Wasser und die Wände der Testzelle einheitliche Temperaturen. Anschließend wird die Temperatur einer vertikalen Wand schlagartig auf 0°C abgesenkt und konstant gehalten. Die warmen Seitenwände werden während des Versuchs konstant auf Starttemparatur gehalten, die zwischen 8 und 20°C variiert wurde. Die numerische Lösung der Erhaltungsgleichungen wird für alle Experimente diskutiert. Es werden Fotografien der Strömung sowie Berechnungen der Strömungsform vorgestellt. Gemessene und berechnete Temperaturen werden verglichen. Die Ergebnisse belegen einen starken Einfluß der Dichteinversion auf die natürliche Konvektion im Hohlraum. Die Strömungsform läßt sich nicht durch die klassischen Gleichungen für die natürliche Konvektion mit der Boussinesq-Näherung beschreiben.

НЕСТАЦИОНАРНАЯ ЕСТЕСТВЕННАЯ КОНВЕКЦИЯ ВОДЫ ВБЛИЗИ ЭКСТРЕМУМА ЕЕ БЛОТНОСТИ В ПРЯМОУГОЛЬНОЙ ПОЛОСТИ

Аннотация—Экспериментально и теоретически исследуется нестационарный естественноконвективный теплоперенос для воды вблизи каксимума ее плотности в прямоугольной полости, противоположные вертикальные стенки которой поддерживаются при различных температурах. Определяется влияние инверсии плотности воды, достигающей максимальной величины приблизительно при 4°C. При этом первоначально жидкость в испытательной ячейке поддерживается при постоянной температуре, а затем температура одной из ненагретых вертикальных стенок резко снижается и сохраняется равной 0°C. В ходе экспериментов нагретая стенка поддерживается при постоянной температуре, равной начальной температуре воды, которая изменяется от 8 до 20°C. Получены численные решения уравнений для всех обсуждаемых экспериментов. Представлены фотографии, полученные при визуализации течения, и результаты расчетов картин течения, проводится также сравнение измеренных и рассчитанных температур. На основе полученных результатов показано, что инверсия плотности воды оказывает существенное влияние на естественную конвекцию в полости и структуру течения нельзя определить с помощью классических моделей естественной конвекции, использующих приближение Буссинеска.